Journal of Power Sources 218 (2012) 15–20

Contents lists available at SciVerse ScienceDirect

Journal of Power Sources

journal homepage: www.elsevier.com/locate/jpowsour

# *In-situ* investigation of vanadium ion transport in redox flow battery

Qingtao Luo [a], Liyu Li [b], Zimin Nie [a], Wei Wang [a,*], Xiaoliang Wei [a], Bin Li [a], Baowei Chen [a], Zhenguo Yang [b]

[a] *Pacific Northwest National Laboratory, P.O. Box 999, Richland, WA 99354, USA*
[b] *UniEnergy Technologies, LLC, 4333 Harbour Pointe Blvd SW, Unit A, Mukilteo, WA 98275, USA*

## HIGHLIGHTS

- *In-situ* study of the transport behavior of V ions during flow battery operation.
- $VO^{2+}/VO_2^+||Fe^{3+}/Fe^{2+}$ and $Fe^{2+}/Fe^{3+}||V^{3+}/V^{2+}$ flow batteries were constructed for *in-situ* measurement.
- A simplified mathematical model to simulate the vanadium ion transport.

## GRAPHICAL ABSTRACT

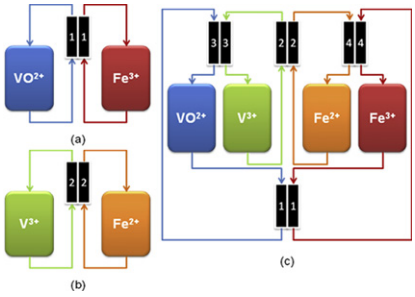


## ARTICLE INFO

*Article history:*
Received 21 May 2012
Received in revised form
16 June 2012
Accepted 18 June 2012
Available online 27 June 2012

*Keywords:*
Vanadium
Transport
Diffusion
Migration
Redox flow battery

## ABSTRACT

Flow batteries with vanadium and iron redox couples as the electroactive species are employed to investigate the transport behavior of vanadium ions in the presence of an electric field. It is shown that the electric field accelerated the positive-to-negative and reduced the negative-to-positive transport of vanadium ions in the charging process and affected the vanadium ion transport in the opposite way during discharge. In addition, a method is designed to differentiate the concentration-gradient-driven vanadium ion diffusion and electric-field-driven vanadium ion migration. A simplified mathematical model is established to simulate the vanadium ion transport in real charge–discharge operation of the flow battery. The concentration gradient diffusion coefficients and electric-migration coefficients of $V^{2+}$, $V^{3+}$, $VO^{2+}$, and $VO_2^+$ across a NAFION® membrane are obtained by fitting the experimental data.



## 1. Introduction

The demand for stationary energy storage has rapidly changed the worldwide landscape of energy system research [1,2], which has brought redox flow battery technology into the spotlight in recent years because it can provide large-scale energy storage to support a more intelligent, efficient, and capable electrical grid system [3,4]. Redox flow battery (RFB) systems are hailed as one of the most promising technologies to be utilized not only for integrating renewable energy resources, but also to improve the efficiency of grid transmission and distribution. Among the different RFB systems, the all-vanadium redox flow battery (VRB) is probably the most promising and extensively researched flow battery system [5–8]. Capitalizing on four different oxidation states of vanadium ions to form two redox couples, VRBs are capable of converting electrical energy to chemical energy and subsequently releasing it in a controlled fashion when needed. Unlike traditional solid-state rechargeable batteries, VRBs store energy in the electrolyte contained in external tanks, while the energy conversion takes place in electrode compartments. As a result, the energy capacity and

* Corresponding author. Tel.: +1 509 372 4097; fax: +1 509 375 2186.
*E-mail address:* wei.wang@pnnl.gov (W. Wang).

0378-7753/$ – see front matter © 2012 Elsevier B.V. All rights reserved.
http://dx.doi.org/10.1016/j.jpowsour.2012.06.066

power capability of a VRB can be varied independently by adjusting the stack size and electrolyte volume accordingly for different power and energy storage applications. Due to its unique mechanism and compelling characteristics such as quick response and long cycle life, among others, VRB technology has sparked considerable research interest in developing electrochemical energy storage technologies for various grid applications such as load-leveling/peak shaving, emergency power backup, and renewable energy integration [9].

The ion exchange membrane (IEM) is one of the most important components in a RFB system; it prevents the crossover of the active materials in the positive and negative electrolytes while supporting proton transport to complete the circuit. Perfluorinated polymer membranes (e.g., NAFION® membranes) have become the choice of IEMs for VRBs due to their high conductivity and excellent chemical stability in highly oxidizing positive electrolytes [10,11]. However, even with perfluorinated membranes such as NAFION 117 [12], NAFION 212 [13], and GORE-SELECT® membranes [14], several groups have reported severe capacity decay of VRBs during cycling. Although the capacity fading mechanism is not entirely understood by the VRB research community, the inevitable crossover of vanadium ions across the membrane may play a significant role in causing the capacity fading during cycling [15]. More seriously, precipitation may occur if the vanadium ion concentration in positive electrolytes continues to increase as a result of the net transfer of vanadium ions [16]. Therefore, it is of great importance to investigate the transport behaviors of vanadium ions across the membrane, which may also shed light on the VRB capacity fading mechanism. The reactions between transported vanadium ions and native vanadium ions, however, make this study very challenging. Previous literature reports either focused on the *ex-situ* static dialysis test or the long term accumulated effect of the vanadium ion transport [15,17,18]. Without the presence of an electric field, the *ex-situ* static dialysis test cannot possibly reveal the complete transport phenomenon of the vanadium ions in real VRB operation. On the other hand, detailed vanadium ion transport information at different states of charge (SOCs) cannot be obtained from the long-term investigation.

In this paper, redox flow batteries with vanadium and iron redox couples were constructed to investigate the transport behaviors of vanadium ions. A $VO^{2+}/VO_2^+||Fe^{3+}/Fe^{2+}$ redox flow battery with $VO^{2+}/VO_2^+$ couples and $Fe^{3+}/Fe^{2+}$ couples as positive and negative active species was employed to study the transport of $VO^{2+}/VO_2^+$. Similarly, the transport of $V^{3+}/V^{2+}$ was investigated by using a $Fe^{2+}/Fe^{3+}||V^{3+}/V^{2+}$ redox flow battery with $Fe^{3+}/Fe^{2+}$ couples and $V^{3+}/V^{2+}$ couples as positive and negative active species. Furthermore, a new method was designed to differentiate the concentration-gradient-driven vanadium ion diffusion and electric-field-driven vanadium ion migration. A simplified Nernst–Planck equation was established to describe the vanadium ion transport behaviors in real operation of flow batteries. Diffusion coefficients and electric-migration coefficients of $VO_2^+$, $VO^{2+}$, $V^{3+}$, and $V^{2+}$ were obtained by fitting the experimental data.

## 2. Experimental

Devices used in these tests included in-house designed single cells, peristaltic pumps (Cole Parmer, Masterflex® *L/S*® 7551), Pyrex® glass beakers as electrolyte reservoirs, and Viton® tubing. Graphite felts (GFD 5, SGL Carbon Group, Germany) with apparent area of 10 $cm^2$ were used as electrodes and NAFION® 115 as membranes in all single cells. Original electrolytes used in these tests included trivalent vanadium electrolyte (1 mol $L^{-1}$ $V^{3+}$ in 5 mol $L^{-1}$ total $Cl^-$), tetravalent vanadium electrolyte (1 mol $L^{-1}$ $VO^{2+}$ in 5 mol $L^{-1}$ total $Cl^-$), trivalent iron electrolyte (1 mol $L^{-1}$ $Fe^{3+}$ in 5 mol $L^{-1}$ total $Cl^-$), and bivalent iron electrolyte, (1 mol $L^{-1}$ $Fe^{2+}$ in 5 mol $L^{-1}$ total $Cl^-$). Trivalent vanadium electrolyte, trivalent iron electrolyte and bivalent iron electrolyte were prepared by dissolving $VCl_3$ (Sigma–Aldrich, 97%), $FeCl_2$ (Sigma–Aldrich, 98%), and $FeCl_3$ (Sigma–Aldrich, 98%) in concentrated HCl (Sigma–Aldrich, 37%) at room temperature. Tetravalent vanadium electrolyte was made by electrochemically charging the trivalent vanadium electrolyte. During the operation of flow batteries, electrolytes inside the reservoirs were circulated in two separate loops through the electrode compartments at a flow rate of 20 mL $min^{-1}$. The reservoir with trivalent vanadium electrolyte was bubbled with nitrogen for 10 min and sealed before testing to prevent $V^{2+}$ from being oxidized to $V^{3+}$. A potentiostat/galvanostat (Arbin Inst., College Station, TX) was employed to carry out the charge–discharge process. Inductively coupled plasma (ICP, Optima 7300DV, Perkin Elmer), was used to measure the total concentration of vanadium ions, including $VO^{2+}$, $VO_2^+$, $V^{3+}$, and $V^{2+}$, in each sample.

Fig. 1 is the schematic diagram of flow batteries for measuring the vanadium ion transport in real charge–discharge operation. In the $VO^{2+}/VO_2^+||Fe^{3+}/Fe^{2+}$ flow battery (Fig. 1(a)), 50 mL tetravalent vanadium electrolyte and 50 mL trivalent iron electrolyte were used as original positive and negative electrolytes, respectively. The battery was charged to 90% SOC and then discharged to 10% SOC. At each interval of 10% SOC change, a 1 mL sample was withdrawn from the negative electrolyte after the potentiostat/galvanostat program and the pump were paused. In order to minimize the change of negative electrolyte composition and volume, 1 mL pre-prepared $Fe^{2+}/Fe^{3+}$ mixed solution with calculated negative electrolyte composition at each SOC was added back to the electrolyte reservoir. The withdrawn samples were subjected to ICP analysis to determine the total vanadium ion concentration. The same procedure was applied to the $Fe^{2+}/Fe^{3+}||V^{3+}/V^{2+}$ flow battery shown in Fig. 1(b). In this case, the original positive and negative electrolytes were 50 mL bivalent iron electrolyte and 50 mL trivalent vanadium electrolyte, and the samples were withdrawn from the positive electrolytes instead of the negative electrolytes.

A flow battery's configuration, as illustrated in Fig. 1(c), was designed to measure the vanadium ion diffusion driven only by concentration gradient. 50 mL tetravalent vanadium electrolyte, 50 mL trivalent vanadium electrolyte, 50 mL bivalent iron electrolyte and 50 mL trivalent iron electrolyte were used as the original electrolytes in reservoirs marked with $VO^{2+}$, $V^{3+}$, $Fe^{2+}$, and $Fe^{3+}$, respectively. Cell 1 and Cell 2 were used as diffusion cells to implement the concentration-gradient-driven vanadium ion diffusion. The SOC changes of all electrolytes were achieved by applying the current to Cell 3 and Cell 4. The procedure for this test was similar to that in the above two tests: electrolytes were charged to 90% SOC and discharged to 10% SOC, and samples were withdrawn from reservoirs marked with $Fe^{2+}$ and $Fe^{3+}$ at each interval of 10% SOC change. Due to the short test time, the changes of total vanadium ion concentration in vanadium-based electrolytes and of total iron ion concentration in iron-based electrolytes were neglected. Vanadium ion transport in this test was the same as that in the above two tests except that there was no electric field across diffusion cells 1 and 2. Vanadium ions transported in iron electrolytes only came from the concentration gradient between the vanadium-based electrolytes and iron-based electrolytes.

## 3. Results and discussion

The test results of vanadium ion transport in a $VO^{2+}/VO_2^+||Fe^{3+}/Fe^{2+}$ flow battery are shown in Fig. 2. At the current density of 25 mA $cm^{-2}$, vanadium ion concentration in negative iron-based electrolytes increased in both the charge and discharge processes,

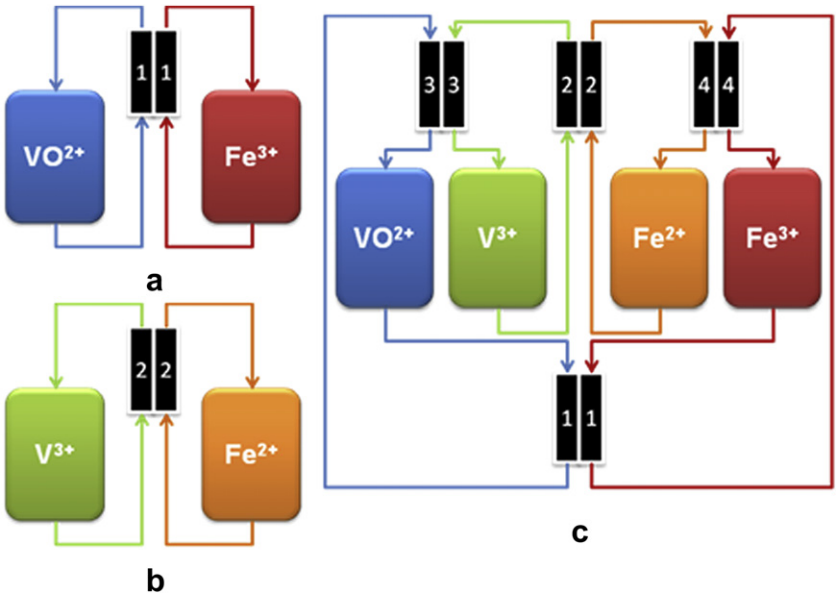


**Fig. 1.** Schematic illustration of the flow cell configuration.

although it was slower in the latter. At the current density of 50 mA $cm^{-2}$, vanadium ion concentration in negative iron-based electrolytes increased as the cell is being charged, but remained relatively constant during the discharge process. The average vanadium ion transport rates in different SOC ranges were calculated and are shown in Fig. 2(b), which clearly demonstrates that the transport of vanadium ions was affected by a combination of different factors, such as the charge/discharge process, current density, and SOC. At both current densities, the vanadium ion transport rate during the charge process is larger than that during discharge. Secondly, with the increase of current density, the vanadium ion transport rate increases during the charge process but decreases during discharge. At each given current density, the vanadium ion transport rate, in general, demonstrated a trend of decreasing with the increase of SOC.

The driving forces of ionic transport across a membrane in the presence of an electric field include not only the concentration gradient, but also the potential gradient (electric field). Ionic diffusion flux driven by concentration gradient is always from a high ionic concentration region to a low ionic concentration region with a magnitude proportional to the ionic concentration gradient. Cation migration flux driven by an electric field is from a high potential region to a low potential region, while anion migration flux is opposite to the potential gradient. The vanadium ion transport in the above test is driven by both the concentration gradient and the potential gradient between positive and negative electrolytes. In the above flow battery, the concentration gradient always drives the vanadium ions to transport from the positive side with high vanadium ion concentration to the negative side with low vanadium ion concentration. However, the direction of potential gradient during the charge process is opposite to that during discharge. In the charge process, $VO^{2+}$ reacts with $H_2O$ to produce $VO_2^+$, $H^+$, and electrons [9] on the positive side while $Fe^{3+}$ is reduced to $Fe^{2+}$ on the negative side. The potential gradient produced by the above electrochemical redox reaction will promote the transport of cations ($H^+$, $VO^{2+}$, $VO_2^+$) from positive to negative electrolytes and suppress the transport of cations ($H^+$, $Fe^{3+}$, $Fe^{2+}$) from negative to positive electrolytes. During discharge, the potential gradient is reversed between positive and negative half-cells, which facilitates the negative-to-positive transport of cations ($H^+$, $Fe^{3+}$, $Fe^{2+}$) while suppressing the positive-to-negative transport of cations ($H^+$, $VO^{2+}$, $VO_2^+$). Consequently, vanadium ion transport with high flux occurs during the charge period and that with low flux occurs during discharge. Furthermore, high current density applied to the battery will lead to a high voltage drop across the membrane. The effect of promoting or suppressing the vanadium ion transport is thus further enhanced under higher

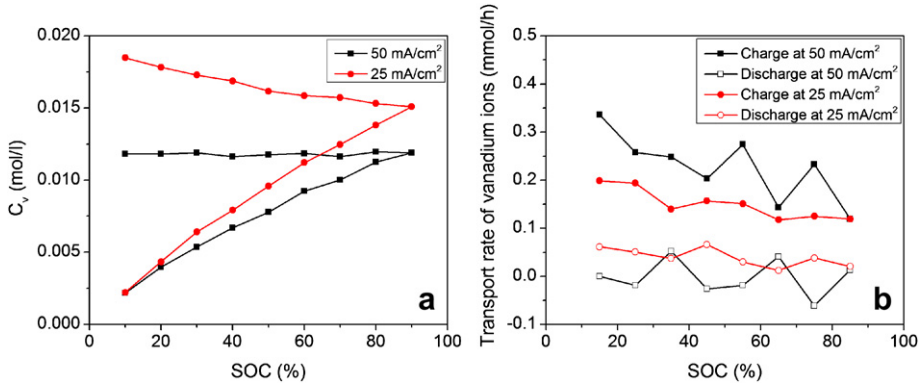


**Fig. 2.** Transport behaviors of $VO^{2+}$, $VO_2^+$ from positive to negative side in one charge–discharge process. (a) Change of vanadium ion concentration in negative half-cell electrolyte with respect to SOC. (b) Average vanadium ion transport rates for a range of SOCs.

current density. As a result, vanadium ion transport flux increases during the charge period and decreases during discharge. On the other hand, SOC is directly related to the ratio between $VO_2^+$ and $VO^{2+}$ ions in the positive half-cell. The change of the vanadium ion transport rate with SOC is believed to originate mainly from different properties of $VO^{2+}$ and $VO_2^+$.

Similar tests were conducted with a $Fe^{2+}/Fe^{3+}||V^{3+}/V^{2+}$ flow battery to investigate the transport behaviors of $V^{3+}/V^{2+}$ using the cell configuration shown in Fig. 1(b). In contrast with the above test, the vanadium ion couple $V^{3+}/V^{2+}$ is in the negative half-cell. Presumably, the effect of the electric field on the transport of vanadium ions is in the opposite direction from the above test due to the change of the vanadium ion transport direction, which was confirmed by comparing the vanadium ion transport behaviors in this test (Fig. 3) to those in the above test (Fig. 2). In this test, the vanadium ion transport rate during the charge process is lower than that during discharge, which demonstrated a trend opposite to Fig. 2. With the increase of current density, the vanadium ion transport rate decreases during the charge process and increases during discharge. The amount of vanadium ion transport after one charge–discharge cycle is larger than that in the test discussed above. With the vanadium ions initially available only in the negative half-cell, the transport in this case is from the negative to the positive side. During the operation of a flow battery, vanadium ion transport will be suppressed during the charge process and promoted during discharge under the influence of the potential gradient. With the increase of current density, the vanadium ion transport flux decreases during the charge process and increases during discharge due to the increase of potential gradient across the membrane. Comparing $VO_2^+$ and $VO^{2+}$ transport in Fig. 2(b) and $V^{2+}$ and $V^{3+}$ transport in Fig. 3(b), the increase of transported vanadium ions during both charge and discharge processes may be caused by the difference in the size and charge number between $V^{2+}$, $V^{3+}$, $VO^{2+}$ and $VO_2^+$ ions. Due to their higher charge numbers and smaller sizes, $V^{2+}$ and $V^{3+}$ permeate more easily through the membrane than the $VO_2^+$ and $VO^{2+}$ ions.

With the same $Fe^{2+}/Fe^{3+}$ solutions as the counter-electrolytes, the obtained $VO^{2+}/VO_2^+$ and $V^{2+}/V^{3+}$ transports were put together to mimic the positive-to-negative and negative-to-positive vanadium ion transports in real VRB operation. The amounts of transported vanadium ions were calculated and summarized in Table 1. As can be seen, the net transfer of vanadium ions is from positive to negative in the charge process and from negative to positive in the discharge process. In a charge–discharge cycle, the net vanadium ion transport is from the negative to the positive side, in good agreement with literature reports [15].

Illustrated in Fig. 1(c) is a flow cell configuration designed to differentiate the driving forces of vanadium ion transport during charge–discharge operation. The setup consisted of four flow cells with Cells 1 and 2 for ion diffusion between vanadium-based electrolytes and iron-based electrolytes, and Cells 3 and 4 for SOC change of electrolytes. With the same current (50 mA $cm^{-2}$) applied to Cells 3 and 4, the change of vanadium ion concentration in vanadium-based electrolytes and iron ion concentration in iron-based electrolytes are the same as those of the two tests previously discussed. However, there is no potential gradient across the membrane in diffusion Cells 1 and 2. As a result, the vanadium ion diffusion from vanadium-based electrolytes to iron-based electrolytes is driven solely by the vanadium ion concentration gradient. The comparison of vanadium ion transport with electric field (previous two tests) and without (this test) is shown in Fig. 4 (the "With electric field" data is re-plotted from the above sections). As can be seen, the transport behaviors of vanadium ions remained largely the same during the charge and discharge processes when there was no electric field between the vanadium-based electrolytes and iron-based electrolytes. While in the presence of an electric field, the transport behaviors of vanadium ions changed dramatically in different stages of the charge–discharge cycle: the transport rate of $VO^{2+}/VO_2^+$ couples is higher during the charge process while that of $V^{3+}/V^{2+}$ couples is higher during the discharge process. From the above comparison, the amount of concentration-gradient-driven vanadium ion diffusion and that of electric-field-driven vanadium ion migration in real operation of flow batteries can be obtained.

In order to understand the vanadium ion transport phenomenon, a simplified model was established to simulate the vanadium ion transport in a real charge–discharge process. Ionic transport flux across the membrane in the presence of an electric field can be described by means of the Nernst–Planck equation [19],

**Table 1**
Amount of vanadium ions transported in a charge–discharge cycle.

| Period | Diffusion of vanadium ions | Amount of transferred vanadium ions (mmol) | |
|---|---|---|---|
| | | 25 mA $cm^{-2}$ | 50 mA $cm^{-2}$ |
| Charge process | Positive to negative | 0.4740 | 0.3645 |
| | Negative to positive | 0.4565 | 0.1750 |
| | Net transfer (N to P) | −0.0175 | −0.1895 |
| Discharge process | Positive to negative | 0.1255 | −0.0085 |
| | Negative to positive | 1.3755 | 1.0890 |
| | Net transfer (N to P) | 1.2500 | 1.0975 |
| Charge–discharge cycle | Positive to negative | 0.6745 | 0.3915 |
| | Negative to positive | 2.1485 | 1.4755 |
| | Net transfer (N to P) | 1.2325 | 0.9080 |

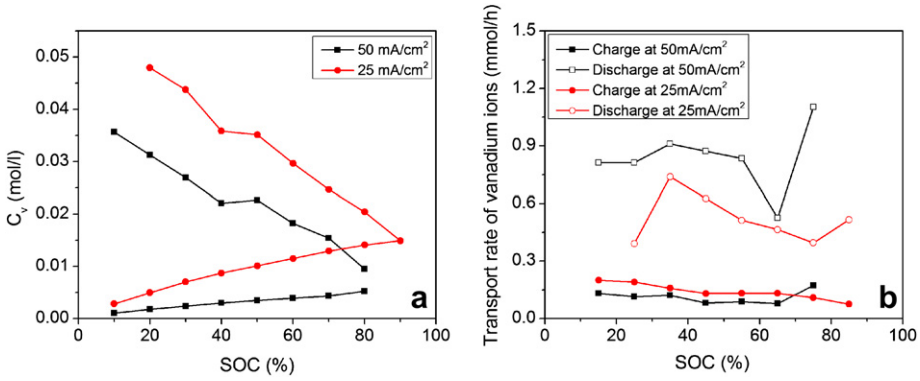


**Fig. 3.** Transport behaviors of $V^{2+}$, $V^{3+}$ from negative to positive side in a charge–discharge cycle. (a) Change of vanadium ion concentration in positive iron electrolytes with respect to SOC. (b) Average vanadium ion transport rate at different SOCs.

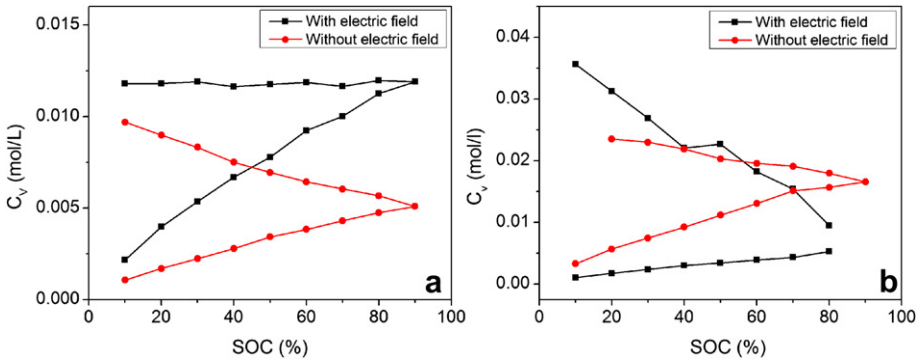


**Fig. 4.** Transport behaviors of vanadium ions with and without electric field. (a) Vanadium ion transport from $VO^{2+}/VO_2^+$ side to $Fe^{3+}/Fe^{2+}$ side with respect to SOC. (b) Vanadium ion diffusion from $V^{3+}/V^{2+}$ side to $Fe^{2+}/Fe^{3+}$ side with respect to SOC.

$$J_i = -D_i\left(\frac{dc_i}{dx} - z_i c_i \frac{FE}{RT}\right) \quad (1)$$

where $J_i$, $D_i$, $c_i$, and $z_i$ denote the flux, the diffusion coefficient, the concentration and the valency of the ion i in the membrane; $x$ stands for the position along the diffusion zone, $E$ denotes the electric field, $F$ the Faraday constant, and $RT$ the universal gas constant times absolute temperature. The following assumptions are made:

1. The change of electrolyte volumes can be neglected due to the short test time.
2. Self-discharge reactions of vanadium ions and iron ions occur in electrolytes instead of in the membrane;
3. The vanadium ion concentration gradient in the membrane was replaced by the ratio of vanadium ion concentration difference between the vanadium and iron electrolytes and the thickness of the membrane, $l$. The vanadium ion concentration in iron electrolytes can be neglected in term of calculating the concentration difference:

$$\frac{dc_i}{dx} = \frac{\Delta C_i}{l} = \frac{C_i}{l} \quad (2)$$

4. The vanadium ion concentration in the membrane is directly related to the vanadium ion concentration in vanadium-based electrolytes:

$$c_i = f(K, C_i) = kC_i \quad (3)$$

5. The electric field in the membrane is constant and equal to the potential drop across the membrane:

$$E = \frac{\Delta V}{l} = \frac{IR_m}{l} \quad (4)$$

In the above equations, $l$ and $R_m$ represent the thickness and resistance of membrane, respectively, while $C_i$, $K$, $k$, $\Delta V$, and $I$ are the concentration of ions i in electrolytes, ion exchange equilibrium constant of ions between electrolytes and membrane, a constant, the voltage drop across the membrane, and the current across the membrane, respectively.

By substituting Eqs. (2)–(4) into Eq. (1), the mathematical model for vanadium ion diffusion can be obtained in the following equation:

$$\frac{dn_i(t)}{dt} = AJ_i = D_i\frac{A}{l}C_i \pm z_i I\frac{FAR_m k}{RTl}C_i = D_i\frac{A}{l}C_i \pm z_i I D_i' C_i \quad (5)$$

In Eq. (5), $A$ represents the area of membrane and $D_i'$ was introduced and defined as electric-migration coefficients. It is related to the thickness, resistance, and ion exchange equilibrium constant of the membrane. For the transport of $VO^{2+}/VO_2^+$ couples, '+' and '−' were used in the charge and discharge processes, respectively. For the transport of $V^{3+}/V^{2+}$ couples, the situation was reversed: '+' was used in discharge process and '−' in the charge process.

In the absence of an electric field, the vanadium ion diffusion came only from the concentration gradient. The vanadium ion diffusion can be expressed as:

$$\frac{dn(t)}{dt} = \frac{A}{L}(D_i C_i + D_j C_j) \quad (6)$$

In the presence of an electric field, the vanadium ion transport came from the combination of concentration-gradient-driven diffusion and electric potential-gradient-driven migration. The vanadium ion transport can be expressed as:

$$\frac{dn(t)}{dt} = \frac{A}{L}(D_i C_i + D_j C_j) + I\left(z_i D_i' C_i + z_j D_j' C_j\right) \quad (7)$$

Here, subscripts i, j are designated for $V^{3+}$, $V^{2+}$ with negative vanadium ion transport and $VO^{2+}$, $VO_2^+$ with positive vanadium ion transport. Based on the test data in Fig. 4, the concentration gradient diffusion coefficients $D_i$ and electric-migration coefficients $D_i'$ of vanadium ions were calculated by fitting the experimental data and listed in Table 2. The vanadium ion transport in a $VO^{2+}/VO_2^+ \| Fe^{3+}/Fe^{2+}$ and $Fe^{2+}/Fe^{3+} \| V^{3+}/V^{2+}$ battery at different operation conditions can be simulated on the basis of the above model and the coefficients. As shown in Fig. 5, the simulated values of vanadium ion transport at the current density of 25 mA $cm^{-2}$ match very well with the experimental data.

In summary, $VO^{2+}/VO_2^+ \| Fe^{3+}/Fe^{2+}$ and $Fe^{2+}/Fe^{3+} \| V^{3+}/V^{2+}$ flow batteries were used to investigate the positive-to-negative and negative-to-positive vanadium ion transport in real operation of flow batteries. It is demonstrated that an electric field promotes the positive-to-negative and suppresses the negative-to-positive vanadium ion diffusion during the charge process, while the trend is reversed in the discharge process. With an in-house designed cell

**Table 2**
Concentration gradient-diffusion coefficients and electric-migration coefficients of different vanadium ions across NAFION 115 membrane.

| | $VO_2^+$ | $VO^{2+}$ | $V^{3+}$ | $V^{2+}$ |
|---|---|---|---|---|
| $D_i$ ($10^{-6}$ $cm^2$ $min^{-1}$) | 1.442 | 2.667 | 8.668 | 5.661 |
| $D_i'$ ($10^{-3}$ $cm^3$ $min^{-1}$ $A^{-1}$) | 2.098 | 3.300 | 2.967 | 3.146 |

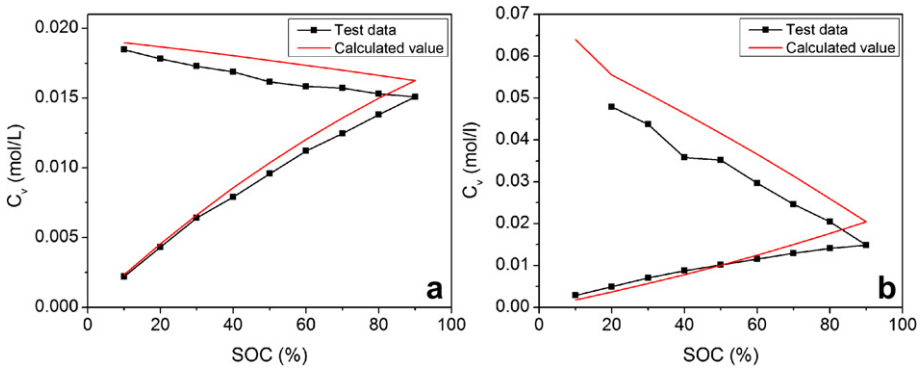


**Fig. 5.** Comparison between calculated and measured vanadium ion transport at the current density of 25 mA $cm^{-2}$. (a) Vanadium ion transport from $VO^{2+}/VO_2^+$ side to $Fe^{3+}/Fe^{2+}$ side. (b) Vanadium ion transport from $V^{3+}/V^{2+}$ side to $Fe^{2+}/Fe^{3+}$ side.

configuration, the concentration-gradient-driven vanadium ion diffusion in real operation of flow batteries was determined. The concentration-gradient-driven vanadium ion diffusion and electric-field-driven vanadium ion migration can be differentiated by comparing the vanadium ion transport with and without an electric field. A simplified mathematical model was established to simulate the vanadium ion transport, and the concentration-gradient diffusion coefficients and electric-migration coefficients were calculated on the basis of experimental data.

With the growing interest in developing VRB systems for large-scale grid energy storage, it is a pressing task to tackle the lingering capacity fading issue in VRB systems, which clearly underscores the need for greater comprehension of the transport phenomena during VRB operation. The construction of $VO^{2+}/VO_2^+||Fe^{3+}/Fe^{2+}$ and $Fe^{2+}/Fe^{3+}||V^{3+}/V^{2+}$ flow batteries reported in this paper renders a unique opportunity to study for the first time the transport behavior of vanadium ions in a circumstance imitating real VRB operation. Although the diffusion environment and electric field strength within $VO^{2+}/VO_2^+||Fe^{3+}/Fe^{2+}$ and $Fe^{2+}/Fe^{3+}||V^{3+}/V^{2+}$ flow batteries are clearly different from those in a true VRB, this innovative method undoubtedly affords a new avenue to explore the ion transport behavior of the VRB, and RFBs in general. Advances in understanding of the ion transport mechanism during RFBs operation will provide insights and prompt strategies to circumvent the capacity decay, which is of paramount importance to the long-term operation stability of RFBs for the grid application.

## 4. Conclusion

The vanadium ion transport behaviors including diffusion and migration were investigated with an in-house designed vanadium and iron redox flow cell. The concentration gradient diffusion coefficients and electric-migration coefficients of the vanadium ions with different valence were obtained through a simple mathematical model fitting the experiment data.

## Acknowledgements

The authors would like to acknowledge financial support from the U.S. Department of Energy's (DOE's) Office of Electricity Delivery & Energy Reliability (OE) (under Contract No. 57558). We are also grateful for useful discussions with Dr. Imre Gyuk of the DOE-OE Grid Storage Program. Pacific Northwest National Laboratory is a multi-program national laboratory operated by Battelle for DOE under Contract DE-AC05-76RL01830.

## References

[1] B. Dunn, H. Kamath, J.-M. Tarascon, Science 334 (2011) 928–935.
[2] Z. Yang, J. Zhang, M.C.W. Kintner-Meyer, X. Lu, D. Choi, J.P. Lemmon, J. Liu, Chem. Rev. 111 (2011) 3577–3613.
[3] M. Skyllas-Kazacos, M.H. Chakrabarti, S.A. Hajimolana, F.S. Mjalli, M. Saleem, J. Electrochem. Soc. 158 (2011) R55–R79.
[4] A. Weber, M. Mench, J. Meyers, P. Ross, J. Gostick, Q. Liu, J. Appl. Electrochem. 41 (2011) 1137–1164.
[5] E. Sum, M. Rychcik, M. Skyllas-kazacos, J. Power Sources 16 (1985) 85–95.
[6] E. Sum, M. Skyllas-Kazacos, J. Power Sources 15 (1985) 179–190.
[7] M. Skyllas-Kazacos, M. Rychcik, R.G. Robins, A.G. Fane, M.A. Green, J. Electrochem. Soc. 133 (1986) 1057–1058.
[8] M. Skyllas-Kazacos, M. Rychick, R. Robins, in: US Patent 4,786,567, 1988.
[9] L. Li, S. Kim, W. Wang, M. Vijayakumar, Z. Nie, B. Chen, J. Zhang, G. Xia, J. Hu, G. Graff, J. Liu, Z. Yang, Adv. Energy Mater. 1 (2011) 394–400.
[10] Q. Luo, H. Zhang, J. Chen, D. You, C. Sun, Y. Zhang, J. Membr. Sci. 325 (2008) 553–558.
[11] X. Li, H. Zhang, Z. Mai, H. Zhang, I. Vankelecom, Energy Environ. Sci. 4 (2011).
[12] S. Kim, J. Yan, B. Schwenzer, J. Zhang, L. Li, J. Liu, Z. Yang, M.A. Hickner, Electrochem. Commun. 12 (2010) 1650–1653.
[13] C. Jia, J. Liu, C. Yan, J. Power Sources 195 (2010) 4380–4383.
[14] T. Sukkar, M. Skyllas-Kazacos, J. Appl. Electrochem. 34 (2004) 137–145.
[15] C. Sun, J. Chen, H. Zhang, X. Han, Q. Luo, J. Power Sources 195 (2010) 890–897.
[16] M. Vijayakumar, L. Li, G. Graff, J. Liu, H. Zhang, Z. Yang, J.Z. Hu, J. Power Sources 196 (2011) 3669–3672.
[17] E. Wiedemann, A. Heintz, R.N. Lichtenthaler, J. Membr. Sci. 141 (1998) 215–221.
[18] E. Wiedemann, A. Heintz, R.N. Lichtenthaler, J. Membr. Sci. 141 (1998) 207–213.
[19] V.M. Aguilella, S. Mafé, J. Pellicer, Electrochim. Acta 32 (1987) 483–488.